Structure of the Ni Sites in Hydrogenases by X-ray Absorption Spectroscopy. Species Variation and the Effects of Redox Poise

Zhijie Gu,[†] Jun Dong,[‡] Christian B. Allan,[†] Suranjan B. Choudhury,[†] Ricardo Franco,[§] José J. G. Moura,[§] Isabel Moura,[§] Jean LeGall,[‡] Alan E. Przybyla,[‡] W. Roseboom,[⊥] Simon P. J. Albracht,[⊥] Milton J. Axley,[∥] Robert A. Scott,*[,‡] and Michael J. Maroney*[,†,▽]

Contribution from the Department of Chemistry, University of Massachusetts, Amherst, Massachusetts 01003, Departamento de Química (and Centro de Química Fina e Biotecnologia), Faculdade de Ciências, Universidade Nova de Lisboa, 2825 Monte de Caparica, Lisboa, Portugal, Center for Metalloenzyme Studies, University of Georgia, Athens, Georgia 30602-2556, E. C. Slater Institute, Biochemistry /FS, University of Amsterdam, Plantage Muidergracht 12, NL-1018 TV Amsterdam, The Netherlands, and National Naval Medical Center, Naval Medical Research Institute, Bethesda, Maryland 20889-5055

Received July 15, 1996[⊗]

Abstract: Structural information obtained from the analysis of nickel K-edge X-ray absorption spectroscopic data of [NiFe]hydrogenases from *Desulfovibrio gigas, Thiocapsa roseopersicina, Desulfovibrio desulfuricans* (ATCC 27774), *Escherichia coli* (hydrogenase-1), *Chromatium vinosum,* and *Alcaligenes eutrophus* H16 (NAD⁺-reducing, soluble hydrogenase), poised in different redox states, is reported. The data allow the active-site structures of enzymes from several species to be compared, and allow the effects of redox poise on the structure of the nickel sites to be examined. In addition, the structure of the nickel site obtained from recent crystallographic studies of the *D. gigas* enzyme (Volbeda, A.; Charon, M.-H.; Piras, C.; Hatchikian, E. C.; Frey, M.; Fontecilla-Camps, J. C. *Nature* **1995,** *373,* 580−587) is compared with the structural features obtained from the analysis of XAS data from the same enzyme. The nickel sites of all but the oxidized (as isolated) sample of *A. eutrophus* hydrogenase are quite similar. The nickel K-edge energies shift 0.9−1.5 eV to lower energy upon reduction from oxidized (forms A and B) to fully reduced forms. This value is comparable with no more than a one-electron metal-centered oxidation state change. With the exception of *T. roseopersicina* hydrogenase, most of the edge energy shift (~0.8 eV) occurs upon reduction of the oxidized enzymes to the EPR-silent intermediate redox level (SI). Analysis of the XANES features assigned to 1s → 3d electronic transitions indicates that the shift in energy that occurs for reduction of the enzymes to the SI level may be attributed at least in part to an increase in the coordination number from five to six. The smallest edge energy shift is observed for the *T. roseopersicina* enzyme, where the XANES data indicate that the nickel center is always six-coordinate. With the exception of the oxidized sample of *A. eutrophus* hydrogenase, the EXAFS data are dominated by scattering from S-donor ligands at ~2.2 Å. The enzyme obtained from *T. roseopersicina* also shows evidence for the presence of O,N-donor ligands. The data from *A. eutrophus* hydrogenase are unique in that they indicate that a significant structural change occurs upon reduction of the enzyme. EXAFS data obtained from the oxidized (as isolated) *A. eutrophus* enzyme indicate that the EXAFS is dominated by scattering from 3−4 N,O-donor atoms at 2.06(2) Å, with contributions from 2−3 S-donor ligands at 2.35(2) Å. This changes upon reduction to a more typical nickel site composed of ~4 S-donor ligands at a Ni−S distance of 2.19(2) Å. Evidence for the presence of atoms in the 2.4−2.9 Å distance range is found in most samples, particularly the reduced enzymes (SI, form C, and R). The analysis of these data is complicated by the fact that it is difficult to distinguish between S and Fe scattering atoms at this distance, and by the potential presence of both S and another metal atom at similar distances. The results of EXAFS analysis are shown to be in general agreement with the published crystal structure of the *D. gigas* enzyme.

Introduction

Redox transformation of dihydrogen to protons and vice versa is of central importance to the metabolism of a large variety of microorganisms.[1] H₂ can be oxidized, providing a source of high-energy reducing equivalents, or can be generated as a repository for excess electrons.[2,3] The vectorial use of this enzymology may represent an ancient mechanism for the generation of proton gradients.[2] The reversible two-electron oxidation of H₂ is carried out by a diverse family of enzymes known as hydrogenases, which can be categorized on the basis of their cofactor content as [Fe]- or [NiFe]hydrogenases.[4,5] A few of the latter hydrogenases contain essential Se in the form of selenocysteine which replaces a conserved cysteine.[6] The recent discovery of a quasi-hydrogenase (the purified enzyme

† University of Massachusetts.
‡ University of Georgia.
§ Universidade Nova de Lisboa.
⊥ University of Amsterdam.
∥ Naval Medical Research Institute.
▽ Phone: (413) 545-4876. FAX: (413) 545-4490. E-mail: MMaroney@chem.UMass.edu.

(1) Hausinger, R. P. *Microbiol. Rev.* **1987,** *51,* 22−42.
(2) Przybyla, A. E. *FEMS Microbiol. Rev.* **1992,** *8,* 109−135.
(3) Hausinger, R. P. *Microbiol. Rev.* **1987,** *51,* 22−42.
(4) Albracht, S. P. J. *Biochim. Biophys. Acta* **1994,** *1188,* 167−204.
(5) Adams, M. W. W. *Biochim. Biophys. Acta* **1990,** *1020,* 115−145.

cannot activate hydrogen) involved in the reduction of methylenetetrahydromethanopterin that contains no metal cofactors[7] suggests that this categorization may be only partially successful.

[NiFe]hydrogenases are by far the most common type of enzyme and are found in both strictly and facultatively anaerobic microorganims (in which the ultimate electron acceptor can be CO_2, SO_4^{2-}, NO_3^-, or fumarate), as well as in aerobic microorganisms (where the ultimate electron acceptor is O_2).[2,3] Autotrophic, chemolithotrophic, and phototrophic microorganisms from both the bacterial and archaeal domains utilize [NiFe]-hydrogenases.[2,3,8] The presence of a "large" subunit that contains N-terminal R-X-C-X_2-C and C-terminal D-P-C-X_2-C motifs that provide the ligands to the Ni-containing H_2-activation site[9] is the defining feature of the [NiFe]hydrogenase family.[2,4] Other subunits that provide the "redox connections" to the immediate environment can vary widely from source to source or may not be part of the purified hydrogenase.[4] In our studies, we have used the technique of X-ray absorption spectroscopy (XAS) to compare and contrast the Ni active-site structures of [NiFe]hydrogenases from a variety of sources. XAS also provides information concerning the effects of enzyme redox state on the Ni active-site electronic structure.

Electron paramagnetic resonance (EPR) spectroscopy has played a crucial role in the discovery[10,11] and study of the Ni active site in the [NiFe]hydrogenases. A series of redox states of the enzyme can be identified based on the observation of EPR signals at 77 K that exhibit ^{61}Ni hyperfine splittings in isotopically labeled samples.[12-17] As aerobically isolated, EPR signals corresponding to oxidized and catalytically inactive forms of the enzyme are typically observed (forms A and B).[18] The two oxidized forms may be distinguished by their EPR spectra and kinetics of reductive activation. Form A ($g = 2.32$, 2.23, 2.01) corresponds to an oxidized form of the enzymes that has apparently been reversibly inactivated in air and is only slowly reactivated under reducing conditions; it is often referred to as the "unready" state (Ni_u).[4] Form B ($g = 2.34$, 2.16, 2.01) is also inactive but apparently represents a different conformation of the active site since it is reactivated quickly upon reduction and is often referred to as the "ready" state (Ni_r). Reductive titrations (or H_2 incubation) of these oxidized forms of the enzyme result first in the disappearance of $g \approx 2$ EPR signals (the SI or EPR "silent intermediate" state), followed by

appearance of a third EPR active state, form C ($g = 2.19$, 2.14, 2.01), that represents a redox level associated with active enzyme. Further H_2 incubation eliminates the form C EPR signal, giving rise to the fully reduced enzyme, the Ni site of which we will refer to as R. A few members of the [NiFe]-hydrogenase family do not display the full complement of these EPR signals and/or may be normally isolated in a state that exhibits no EPR signals in the $g = 2-2.3$ region of the spectrum that are due to the active site. These states are generally assumed to be analogous to SI (e.g., the soluble hydrogenase from *Alcaligenes eutrophus*).

The recent 2.85 Å resolution crystallographic analysis of the [NiFe]hydrogenase from *Desulfovibrio gigas* provided surprising evidence for a heterodinuclear active site in which the nickel and another metal, X, tentatively identified as iron, are bridged by two cysteine thiolates and possibly a third unidentified ligand.[9] This active site is buried deeply, along with the processed C-terminal helix, in the large (60 kD) subunit of this heterodimeric protein and the expected cysteine ligands are bound to the nickel in terminal (Cys65 and -530) or bridging (Cys68 and -533) fashion. The redox state of the enzyme in the crystals used in these experiments was determined to be about 50% forms A and B (mostly form A) and 50% EPR-silent, possibly explaining the somewhat disordered nature (large temperature factors) of the structure around the nickel site.[9] The crystallographic results describe a nickel environment that consists of four cysteine thiolate ligands, one of which (Cys533) has a longer Ni–S bond ($\sim$2.6 Å) compared to the others (averaging $\sim$2.25 Å). In addition, another metal resides ca. 2.7 Å away from the nickel and there may be another (presumably non-S) bridging ligand bound to the nickel.[9]

X-ray absorption spectroscopic (XAS) studies have contributed electronic and molecular structural information about the nickel active site of the [NiFe]hydrogenases that are complementary to that obtained by X-ray crystallography. By detecting the effect on the X-ray absorption coefficient of the scattering of the photoelectron generated by dissociation of a Ni 1s electron, Ni K-edge XAS provides structural information on the local environment of the nickel. Nickel–ligand distances can be determined with higher precision (perhaps $\pm$0.02 Å) than available in macromolecular crystal structures. In addition, since the amount of energy required to dissociate a 1s electron is sensitive to the valence electron configuration, XAS provides a measure of the valence electron density of the nickel (and therefore changes in the nickel redox state, assuming an approximately constant ligand environment).

Early experiments using Ni EXAFS to examine [NiFe]-hydrogenases from *D. gigas*[19,20] and *Methanobacterium thermoautotrophicum*[21] determined the Ni coordination environment to consist of predominantly S-containing ligands. Also, Ni and Se EXAFS were used,[22] in addition to EPR,[23] to show that the selenium of the selenocysteine of the [NiFeSe]hydrogenase from *Desulfovibrio baculatus* is bound to the nickel. This selenocysteine occupies a sequence position analogous to Cys530 of

(6) Fauque, G.; Peck, H. D., Jr.; Moura, J. J. G.; Huynh, B. H.; Berlier, Y.; DerVartanian, D. V.; Teixeira, M.; Przybyla, A. E.; Lespinat, P. A.; Moura, I.; LeGall, J. *FEMS Microbiol. Rev.* **1988**, *4*, 299−344.

(7) Zirngibl, C.; Dongen, W. V.; Schworer, B.; Bunau, R. V.; Richter, M.; Klein, A.; Thauer, R. K. *Eur. J. Biochem.* **1992**, *208*, 511−520.

(8) Friedrich, B.; Schwartz, E. *Annu. Rev. Microbiol.* **1993**, *47*, 351−383.

(9) Volbeda, A.; Charon, M.-H.; Piras, C.; Hatchikian, E. C.; Frey, M.; Fontecilla-Camps, J. C. *Nature* **1995**, *373*, 580−587.

(10) Lancaster, J. R. *FEBS Lett.* **1980**, *115*, 285−288.

(11) Lancaster, J. R. *Science* **1982**, *216*, 1324−1325.

(12) LeGall, J.; Ljungdahl, P. O.; Moura, I.; Peck, H. D., Jr.; Xavier, A. V.; Moura, J. J. G.; Teixeira, M.; Huynh, B. H.; DerVartanian, D. V. *Biochem. Biophys. Res. Commun.* **1982**, *106*, 610−616.

(13) Fernandez, V. M.; Hatchikian, E. C.; Cammack, R. *Biochim. Biophys. Acta* **1985**, *832*, 69−79.

(14) Fernandez, V. M.; Hatchikian, E. C.; Patil, D. S.; Cammack, R. *Biochim. Biophys. Acta* **1986**, *883*, 145−154.

(15) Cammack, R.; Patil, D. S.; Hatchikian, E. C.; Fernandez, V. M. *Biochim. Biophys. Acta* **1987**, *912*, 98−109.

(16) Guigliarelli, B.; More, C.; Fournel, A.; Asso, M.; Hatchikian, E. C.; Williams, R.; Cammack, R.; Bertrand, P. *Biochemistry* **1995**, *34*, 4781−4790.

(17) Albracht, S. P.; Graf, E. G.; Thauer, R. K. *FEBS Lett.* **1982**, *140*, 311−3.

(18) Redox states of enzymes designated as "forms" represent cases where the presence of a single Ni site can be demonstrated by EPR spectroscopy (e.g., form A). In the absence of spectral evidence confirming the presence of a single species at a given redox level, the redox levels are indicated but not designated as forms (e.g., SI).

(19) Scott, R. A.; Wallin, S. A.; Czechowski, M.; DerVartanian, D. V.; LeGall, J.; Peck, H. D., Jr.; Moura, I. *J. Am. Chem. Soc.* **1984**, *106*, 6864−6865.

(20) Scott, R. A.; Czechowski, M.; DerVartanian, D. V.; LeGall, J.; Peck, H. D., Jr.; Moura, I. *Rev. Port. Quim.* **1985**, *27*, 67−70.

(21) Lindahl, P. A.; Kojima, N.; Hausinger, R. P.; Fox, J. A.; Teo, B. K.; Walsh, C. T.; Orme-Johnson, W. H. *J. Am. Chem. Soc.* **1984**, *106*, 3062−3064.

(22) Eidsness, M. K.; Scott, R. A.; Prickril, B.; DerVartanian, D. V.; LeGall, J.; Moura, I.; Moura, J. J. G.; Peck, H. D., Jr. *Proc. Natl. Acad. Sci. U.S.A.* **1989**, *86*, 147−151.

(23) He, S. H.; Teixeira, M.; LeGall, J.; Patil, D. S.; Moura, I.; Moura, J. J. G.; DerVartanian, D. V.; Huynh, B. H.; Peck, H. D., Jr. *J. Biol. Chem.* **1989**, *264*, 2678−2682.

the *D. gigas* enzyme. Analysis of the Ni K-edges of the *D. gigas* enzyme showed a slight increase in the electron density at the nickel (i.e., a shift in the Ni edge to lower energy) upon full H_2 reduction,[20,24] whereas more recent extensive analysis of edge shifts for the [NiFe]hydrogenase from *Thiocapsa roseopersicina* revealed a virtually insignificant shift in the Ni K-edge position.[25,26] Ni EXAFS of the *T. roseopersicina* enzyme also revealed a mixed ligand set of N,O- and S-containing ligands.[26] In addition, a scattering atom at a long distance was detected, and fit as a long S-donor ligand in some forms of this enzyme.[25,27]

With the appearance of the first crystallographic information on the Ni-containing active site of a [NiFe]hydrogenase,[9] we felt a comparison of existing and new Ni XAS results on [NiFe]-hydrogenases from a variety of sources would be timely. These results can now also be compared with the existing crystallographic information to help clarify the structural and redox transformations of the active site. Here we compare and contrast Ni XAS data on [NiFe]hydrogenases from *D. gigas*, *T. roseopersicina*, *D. desulfuricans* (ATCC 27774), *Escherichia coli*, *Chromatium vinosum*, and *Alcaligenes eutrophus* H16, poised in different redox states. The study employing *C.vinosum* hydrogenase is only the second study to examine all five redox states defined by the 77 K EPR spectra in a single enzyme. The resulting structural data are then discussed in light of the recent crystal structure.

Experimental Section

Enzyme and XAS Sample Preparations. *Chromatium vinosum* (strain DSM 185) was grown in a 700 L batch culture and the hydrogenase was isolated and purified as previously described.[28] A fully reduced sample, R, was prepared by concentrating a solution of the purified enzyme in 50 mM Tris/HCl buffer (pH 8.0), transferring it to a polycarbonate XAS cuvette, incubating the sample with pure H_2 gas for 30 min at 50 °C, and then freezing it in liquid N_2. A sample of form C was prepared from a similarly prepared sample of R, except at pH 6. Following reduction under pure H_2, the sample was repeatedly evacuated and flushed with 1% H_2 in He. After 30 min at 50 °C, the sample was frozen. A sample of form A was prepared starting from a sample of R (pH 8) in diluted form prior to final concentration. The preparation was then repeatedly evacuated and flushed with CO and left for 30 min, at room temperature. The sample was then cooled in ice and repeatedly evacuated and flushed with pure O_2. After stirring for 10 min, the sample was concentrated, placed in an XAS cuvette, and frozen. A sample of form B was also prepared from a dilute sample of R, except at pH 9. This sample was evacuated and flushed once with Ar, and then flushed a few times with pure O_2. After stirring for 10 min., the sample was concentrated, placed in an XAS cuvette, and frozen. The SI sample employed in these studies was prepared from an as-isolated sample that was 92% form B. The following redox mediators (all 50 μM) were added to the cold, dilute enzyme sample: 2,3,5,6-tetramethyl-*p*-phenylenediamine (TMPD, $E_0' = +275$ mV), 2,6-dichlorophenol−indophenol (DCIP, $E_0' = +230$ mV), phenazine methosulfate (PMS, $E_0' = +80$ mV), methylene blue ($E_0' = +11$ mV), 2-hydroxy-1,4-naphtoquinone ($E_0' = -139/152$ mV), benzyl viologen ($E_0' = -335$ mV). The sample was then concentrated and placed in an XAS cuvette in an Ar atmosphere. After cooling to 4 °C, 15 mM dithiothreitol was added and the EPR spectrum was checked after 60 min at 4 °C. Dithionite was subsequently added to a final concentration

of 50 mM, and the sample was frozen after 30 min at 4 °C. All samples were stored and shipped in liquid N_2. EPR spectra of the XAS samples were taken before and after exposure to synchrotron radiation to confirm the redox poise of the samples. Spectra were obtained at 77 K by using a finger dewar filled with liquid N_2 and either a Varian E-9 or a Bruker ECS 106 X-band EPR spectrometer at a field modulation frequency of 100 kHz.

The samples of hydrogenases from *Desulfovibrio* species were obtained from cells grown as previously described, and were purified by published procedures: *D. gigas* periplasmic hydrogenase;[29] *D. desulfuricans* ATCC 27774 periplasmic hydrogenase.[30] All of the preparations used for XAS data collection had specific activities in agreement with literature values. Each sample was prepared in 0.1 M Tris/HCl buffer (pH 7.6), and had a protein concentration of 0.5−0.6 mM. For native samples, 160 μL of this solution was placed directly into a sample cell via a syringe. The cell was capped and immediately frozen by immersion in liquid N_2. In order to poise the enzymes in redox states different from the native redox states, a system consisting of a capped glass tube (10.5 cm height × 2 cm diameter) containing the protein solution was used. The sample cells were kept inside the glass tube in order not to perturb the atmosphere when transferring a sample from the solution to the cell via a gas-tight syringe. After transferring the sample, the whole system was frozen and the filled cell was removed. The following mediators (80 μM each) were added to the protein solution in order to ensure a homogeneous redox state for each sample: phenazine ethosulfate ($E_0' = +55$ mV), methylene blue ($E_0' = +11$ mV), indigotetrasulfonate ($E_0' = -46$ mV), 2-hydroxy-2,4-naphthoquinone ($E_0' = -145$ mV), anthraquinone-2,7-disulfonate ($E_0' = -182$ mV), safranine T ($E_0' = -289$ mV), benzyl viologen ($E_0' = -335$ mV), methyl viologen ($E_0' = -436$ mV), *m*-triquat bromide ($E_0' = -546$ mV), *m*-dimethyltriquat bromide ($E_0' = -617$ mV). The protein mediator solution was first incubated under ultrapure hydrogen gas (1 atm) for a period of 2−3 h, after which a fully reduced sample could be obtained. The reoxidation of the samples used to obtain the higher redox states of the enzymes was achieved by increasing the partial pressure of Ar and reducing the partial pressure of H_2. Fully reduced samples were alternatively prepared by anaerobic dithionite reduction of native enzyme samples. The redox state of the samples was ascertained by monitoring EPR spectra: The Lucite/Mylar cell was fitted to an EPR tube by means of an adapter, and the EPR spectrum was obtained on a Bruker ESP 380 X-band spectrometer equipped with an Oxford Instruments continuous flow cryostat. All samples were stored in liquid N_2 until the time of data collection.

E. coli hydrogenase-1 was isolated from AP6 cells grown anaerobically at 37 °C in 0.4% glucose. The cells were disrupted with a Gaulin press and treated with 0.001% DNase, and the membranes were collected at 100000g for 1 h. The membrane pellet was extracted twice in a buffer containing 2.0% TritonX-100 and 50 mM Tris, pH 7.2, by gently mixing overnight at 4 °C. The brown extract was dialyzed overnight, passed twice over a Poros IIQP anion exchange column, eluted from a preparative native polyacrylamide gel prepared in a BioRad Prep Cell apparatus (Bio-Rad, Hercules, CA), and purified by hydroxylapatite chromatography. The purified enzyme had a specific activity of 26.5 (units/mg)/min, about twice the previously reported value,[31] and plasma emission spectroscopy determined the metal content to be 0.93 atom of nickel and 11.4 atoms of iron per mole of hydrogenase-1.

The soluble NAD^+-reducing hydrogenase of *Alcaligenes eutrophus* H16 was purified as described previously.[32] Flavin mononucleotide was added to the purified enzyme to a final concentration of 0.1 mM, and the enzyme was then concentrated to 180 mg/mL using an Amicon stirred-cell ultrafiltration device fitted with a 10 kDa molecular weight cutoff membrane. A 150 μL sample of the concentrated enzyme was removed, glycerol was added to a final concentration of 35%, and this

(24) Eidsness, M. K.; Sullivan, R. J.; Scott, R. A. In *Bioinorganic Chemistry of Nickel*; Lancaster, J. R., Ed.; VCH: Deerfield Beach, FL, 1988; pp 73−91.

(25) Whitehead, J. P.; Colpas, G. J.; Bagyinka, C.; Maroney, M. J. *J. Am. Chem. Soc.* **1991**, *113*, 6288−6289.

(26) Bagyinka, C.; Whitehead, J. P.; Maroney, M. J. *J. Am. Chem. Soc.* **1993**, *115*, 3576−3585.

(27) Whitehead, J. P.; Gurbiel, R. J.; Bagyinka, C.; Hoffman, B. M.; Maroney, M. J. *J. Am. Chem. Soc.* **1993**, *115*, 5629−35.

(28) Coremans, J. M. C. C.; van der Zwaan, J. W.; Albracht, S. P. J. *Biochim. Biophys. Acta* **1992**, *1119*, 157−68.

(29) Huynh, B. H.; Patil, D. S.; Moura, I.; Teixeira, M.; Moura, J. J. G.; DerVartanian, D. V.; Czechowski, M. H.; Prickril, B. C.; Peck, H. D., Jr.; LeGall, J. *J. Biol. Chem.* **1987**, *262*, 795−800.

(30) Franco, R.; Moura, I.; LeGall, J.; Peck, H. D., Jr.; Huynh, B. H.; Moura, J. J. G. *Biochim. Biophys. Acta* **1993**, *1144*, 302−8.

(31) Sawers, R. G.; Boxer, D. H. *Eur. J. Biochem.* **1986**, *156*, 265−75.

(32) Keefe, R. G.; Axley, M. J.; Harabin, A. L. *Arch. Biochem. Biophys.* **1995**, *317*, 449−456.

"as-isolated" sample was placed in an XAS cuvette and frozen by dropping into liquid nitrogen. The remainder of the concentrated enzyme was taken into an anaerobic chamber (Coy Laboratory Products, Inc., Grass Lake, MI) and flushed with nitrogen gas for 30 min with occasional agitation to remove oxygen. A 150 μL sample of the nitrogen-flushed enzyme was removed, NADH was added to the sample to a final concentration of 0.15 mM, glycerol was added, and this "NADH-reduced" sample was frozen in an XAS cuvette. The remaining enzyme was flushed with hydrogen gas for 30 min with occasional agitation. A sample of this hydrogen-flushed enzyme was removed, treated with NADH as the previous sample, and frozen as a "H$_2$- and NADH-reduced" sample. This last sample was assumed to be in the R state.

XAS Data Collection and Analysis. Ni K-edge XAS data for *C. vinosum* hydrogenase were collected on beamline X9B at the National Synchrotron Light Source, Brookhaven National Laboratory, during several runs. The samples were contained in polycarbonate holders that allowed collection of XAS and EPR data without thawing the samples. These holders were inserted into slotted aluminium holders that were held near 50 K by using a He displex cryostat for XAS data collection. Data were collected as previously described for *T. roseopersicina* hydrogenase samples[26] under dedicated conditions at ca. 2.58 GeV and 120−300 mA by using a Si(220) double crystal monochromator internally calibrated to the first inflection point of Ni foil (8331.6 eV). This arrangement provides a theoretical resolution of ca. 0.5 eV for the 0.5 mm hutch slit height employed. Harmonic rejection was accomplished with a focusing mirror left flat. X-ray fluorescence data were collected by using a 13-element Ge detector (Canberra). A 4 μs dead time correction was employed in analyzing the data from this detector.

The integrity of the samples after ∼12 h of exposure to synchrotron radiation was monitored in three ways. First, EPR spectra taken before and after exposure were compared. Second, the energy of the Ni K-edge obtained from each sample was monitored on sequential scans. Third, samples were assayed for either H$_2$- evolution activity or H$_2$- uptake activity before and after exposure. The first and second assays monitor the redox poise of the sample before, after and during exposure. None of the samples exhibited a significant change in redox poise or activity.

Ni K-edge XAS data for hydrogenases from *D. gigas*, *D. desulfuricans*, *E. coli*, and *A. eutrophus* were collected on beamline 7-3 at the Stanford Synchrotron Radiation Laboratory with the SPEAR ring running under dedicated conditions at 3.0 GeV and 50−100 mA. Samples were held in 2 × 4 × 25 mm polycarbonate cuvettes covered on one 4 × 25 mm side with thin Mylar adhesive tape. Data were collected on samples held at 10 K in a liquid helium flow cryostat (Oxford) as 21 min scans (16−24 scans per sample). The X-ray beam was monochromated by Bragg reflection from a double-crystal Si(220) monochromator with the entrance slits set to 1 mm vertical aperture, resulting in a resolution of ca. 1 eV. The energy was internally calibrated as described above, and harmonic rejection was achieved by detuning the monochromator crystals to 50% of maximum flux. X-ray fluorescence data were collected using a 13-element intrinsic Ge solid-state detector array. The X-ray beam was attenuated to give a maximum count rate at any individual detector element of ca. 35 000 cps.

Data for the Ni(cyclam)(SPh)$_2$ model compound were collected in transmission mode under the conditions described above by using finely ground sample on several layers of Kapton tape.

The data previously recorded for samples of *T. roseopersicina* hydrogenase[26] were re-analyzed beginning with the summed raw data in a manner consistent with the analysis of data from the other hydrogenase samples included in this study.

The XAS spectra were analyzed in analogy with previously published procedures.[26] Correction of the background and normalization of the spectra, as well as correction for detector efficiencies, absorbance by air and cryostat windows, and the variation with energy of the sample X-ray penetration depth, was made by using standard procedures.[33] For the purposes of comparison, the edge energy is taken to be the energy at a normalized absorbance of 0.5, as was previously employed in the
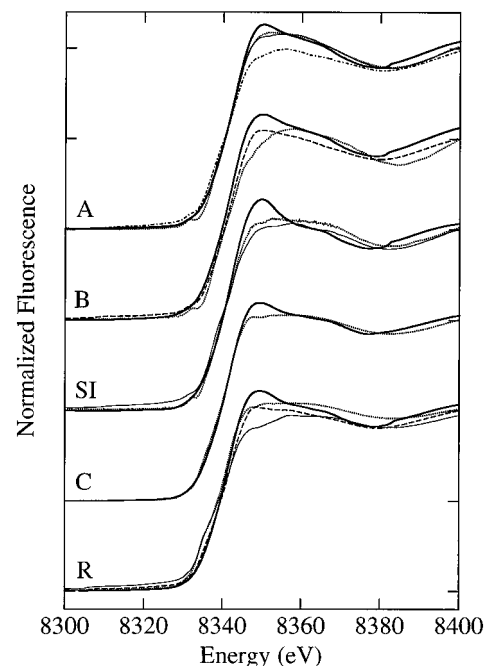
Figure 1. A comparison of the Ni K-edge X-ray absorption spectra for redox-poised samples of hydrogenases from different bacteria in the edge and XANES regions. Spectra are separated by redox level, with line types indicating the different bacterial sources (bold line, *T. roseopersicina*; light line, *D. gigas*; dotted line, *C. vinosum*; dashed line, *D. desulfuricans* ATCC 27774; dashed−dotted line, *E. coli*).

analysis of data from *T. roseopersicina* hydrogenase.[26] The values of the edge energy thus obtained were reproducible to ±0.2 eV. The areas under the peaks assigned to 1s → 3d transitions were determined by fitting a background to the region of the spectrum immediately below and above this feature in energy and integrating the difference. Least-squares fits of the EXAFS data over a k range of 2.0−12.5 Å^{-1} were performed using Fourier-filtered data with a back-transform window of 1.1−2.6 Å (uncorrected for phase shifts). The upper limit of the data was limited in some samples by the presence of trace amounts of Cu in the samples; thus, 12.5 Å^{-1} (8927 eV) was used as an upper limit for all of the data. Best fits were judged by minimizing the goodness of fit criterion (GOF = $[n\{idp\}/(n\{idp\} - n\{p\})]^{1/2}R$, where R = av[(data simulation)/esd(data)], n(p) = the number of varied parameters, and n(idp) = the number of data points for unfiltered refinements or $2(r_{max} - r_{min})(k_{max} - k_{min})/\pi$ for filtered refinements) and the difference in the disorder between model compounds and the fit ($|\Delta\sigma^2| = |(\sigma^2_{fit} - \sigma^2_{model})|$) using single-scattering EXAFS theory (equations 1 and 2).[34] Empirical parameters used in generating the fits (amplitude reduction factors, A, Debye−Waller factors, σ, and values of E_0) were obtained from model compounds.[35]

$$\chi_c = \sum_{shells}\{NA[f(k)]k^{-1}r^{-2}e^{-2\sigma k^2}\sin(2kr + \alpha(k))\} \qquad (1)$$

$$k = [4\pi m_e(E - (8340\ eV + \Delta E))/h]^{1/2} \qquad (2)$$

Results and Discussion

Edges. Figure 1 compares the Ni K-edge X-ray absorption spectra in the XANES region for all hydrogenase samples examined, with the exception of enzyme from *A. eutrophus* (vide infra). This figure compares the shape and position of the edge spectra for samples of a given oxidation state of enzymes from different sources. Table 1 summarizes the edge energy, determined as the position of the normalized edge at half-

(33) Scarrow, R. C.; Maroney, M. J.; Palmer, S. M.; L. Que, J.; Roe, A. L.; Salowe, S. P.; Stubbe, J. *J. Am. Chem. Soc.* **1987**, *109*, 7857−7864.

(34) Scott, R. A. *Methods Enzymol.* **1985**, *117*, 414−459.
(35) Maroney, M. J.; Colpas, G. J.; Bagyinka, C.; Baidya, N.; Mascharak, P. K. *J. Am. Chem. Soc.* **1991**, *113*, 3962−3972.

Table 1. Ni K-Edge and XANES Data for [NiFe]Hydrogenases

redox state	source	edge energy (eV)	1s → 3d area (eV)
form A	*C. vinosum*	8340.0(2)	0.076(5)
	D. gigas	8340.5(2)	0.057(5)
	E. coli	8340.3(2)	0.044(5)
	T. roseopersicina	8340.4(2)	0.015(5)
		av: 8340.3(2)	
form B	*C. vinosum*	8340.4(2)	0.063(5)
	D. desulfuricans	8340.3(2)	0.043(5)
	T. roseopersicina	8339.8(2)	0.016(5)
		av: 8340.2(3)	
SI	*C. vinosum*	8339.6(2)	0.061(5)
	D. gigas	8339.2(2)	0.022(5)
	T. roseopersicina	8339.8(2)	0.014(5)
		av: 8339.5(3)	
form C	*C. vinosum*	8339.4(2)	0.024(5)
	T. roseopersicina	8339.6(2)	<0.001(5)
		av: 8339.5(2)	
R	*C. vinosum*	8339.0(2)	0.011(5)
	D. desulfuricans	8339.6(2)	0.014(5)
	D. gigas	8339.0(2)	0.029(5)
	T. roseopersicina	8339.5(2)	0.007(5)
		av: 8339.3(2)	

Figure 2. Ni K-edge X-ray absorption data for as-isolated (solid line) and NADH- and H_2-reduced (dashed line) samples of the hydrogenase from *A. eutrophus* H16: (a) edge region; (b) Fourier-filtered EXAFS (back-transform window 1.1−2.6 Å); (c) Fourier transform (k^3 weighting, $k = 2.0−12.5$ Å^{-1}).

height,[26,36] for all hydrogenase samples, and also compares the intensities of the 8333 eV 1s → 3d transitions, which provide some indication of nickel site geometry and coordination number.[36]

Examination of the qualitative shape of the Ni XANES spectra in Figure 1 suggests that there may be two different "classes" of edge, one with a higher spectral intensity at ca. 8345 eV (*T. roseopersicina*, *D. desulfuricans*) and the second with a more rounded edge appearance (*D. gigas*, *C. vinosum*, *E. coli*). These edge shapes have been empirically correlated with the types of ligand atoms coordinated to nickel, and the relationships observed suggest a more sulfur-rich nickel environment in the second class.[24,36]

The position of the X-ray absorption edge is a measure of the electron density at the nickel. Metal-based reduction increases the metal valence electron density, shifting the edge position to lower energy. For first-row transition metals, one-electron reduction usually results in a ca. 2 eV shift of the X-ray absorption edge position.[37,38] The data in Table 1 show that the nickel edges of these hydrogenases exhibit shifts of 0.9−1.5 eV to lower energy upon reduction from the form A to the R states. Furthermore, for most enzymes the shift to lower energy occurs mainly upon reduction to the SI state (~0.8 eV) and the edge position changes little upon further reduction to the form C and R states. This suggests that the redox changes responsible for SI → form C → R interconversions do not involve significant electron density changes at the nickel. The magnitude of the edge energy shift that occurs upon reduction to SI is smaller than expected for a metal-centered one-electron reduction.

The intensity of the 8333 eV 1s → 3d transition correlates with nickel-site symmetry and coordination number.[24,36] High-symmetry four-coordinate nickel sites, such as tetrahedral or square planar, are highly unlikely for the hydrogenase active sites examined here. Square-planar Ni(II) complexes exhibit relatively intense transitions at ca. 8336 eV[24] that are not observed in the hydrogenase edges, and tetrahedral Ni(II) complexes exhibit 1s → 3d transitions much more intense than

those observed in the hydrogenase edges. Six-coordinate Ni(II) complexes display peak areas of 0.010−0.040 eV, whereas five-coordinate Ni(II) complexes display peak areas of 0.042−0.096 eV.[36] Table 1 shows that, with the exception of *T. roseopersicina* hydrogenase, the oxidized samples (forms A and B) appear to have five-coordinate nickel sites and the reduced forms (SI, form C, and R) appear to have six-coordinate nickel sites. The conversion from five- to six-coordination occurs between form B and the SI (*e.g.*, *D. gigas*) or form C (*e.g.*, *C. vinosum*) redox states, suggesting that part of the edge energy shift between form A/form B and SI/form C/R may be attributed to edge changes associated with the addition of a sixth ligand (ca. +0.5 eV shift occurs in model complexes upon exchange of a "hard" for a "soft" donor ligand within the same geometry[36]). The hydrogenase from *T. roseopersicina* exhibits both a smaller decrease in edge energy and no apparent coordination number change upon transformation from form A through R. This hydrogenase also exhibits the most distinct edge shape, the edge appearing "sharper" than the others (Figure 1), suggesting more N,O-containing ligands to the nickel site.[24,36]

The Ni XANES spectra for the hydrogenase from *A. eutrophus* behave differently from those for all the other hydrogenases. This enzyme is the only example we have examined of an NAD-requiring hydrogenase and thus, for example, involves a different subunit arrangement than the others.[39] Figure 2a compares the nickel K-edge XANES spectra for as-isolated and NADH- and H_2-reduced forms of this hydrogenase. The as-isolated form of the *A. eutrophus* enzyme is usually EPR-silent,[40] but it is not clear that it is equivalent to the SI states of the other enzymes. The NADH- and H_2-reduced form is probably most closely related to the R states of the other enzymes. The edge of the as-isolated sample is the sharpest of

(36) Colpas, G. J.; Maroney, M. J.; Bagyinka, C.; Kumar, M.; Willis, W. S.; Suib, S. L.; Baidya, N.; Mascharak, P. K. *Inorg. Chem.* **1991**, *30*, 920−928.

(37) Kirby, J. A.; Goodin, D. B.; Wydrzynski, T.; Robertson, A. S.; Klein, M. P. *J. Am. Chem. Soc.* **1981**, *103*, 5537−5542.

(38) Maroney, M. J.; Pressler, M. A.; Mirza, S. A.; Whitehead, J. P.; Gurbiel, R. J.; Hoffman, B. M. *Adv. Chem. Ser.* **1995**, *246*, 21−60.

(39) Friedrich, B.; Schwartz, E. *Annu. Rev. Microbiol.* **1993**, *47*, 351−83.

(40) Cammack, R.; Fernandez, V. M.; Schneider, K. *Biochimie* **1986**, *68*, 85−91.
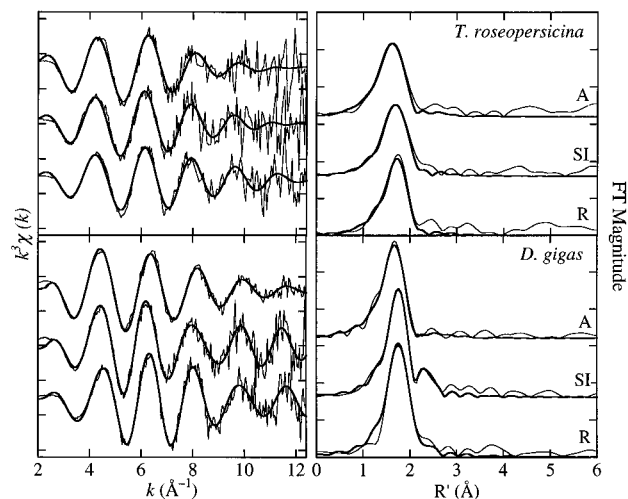
Figure 3. A comparison of Ni EXAFS data of redox-poised hydrogenase samples from *T. roseopersicina* (top) and *D. gigas* (bottom). Bold lines indicate fits from Table 2 (D04, F05, H03, A06, B04, C04).

any, indicating an N,O-rich coordination environment, unlike any of the other hydrogenase Ni sites. The intensity of the 1s → 3d transition (0.056 eV) suggests a five-coordinate site. In addition, Figure 2a shows a significant redox-dependent change in the *A. eutrophus* hydrogenase nickel edge which is not apparent in any of the other enzymes (Figure 1), suggesting a significant nickel-site coordination change upon reduction. The well-resolved shoulder at ca. 8336 eV is reminiscent of Ni(II) sites of distorted square-planar[41] or square-pyramidal (five-coordinate)[36] geometries.

EXAFS. Analysis of the Ni K-edge EXAFS data provides average local structural information about the nickel sites in the hydrogenases. Figure 3 compares EXAFS and Fourier transforms (FTs) of selected oxidation states of the hydrogenases from *T. roseopersicina* and *D. gigas*, two of the best-studied examples. With few exceptions, the EXAFS appear as a single oscillatory pattern giving rise to a single peak in the FT with a phase-shifted distance of ca. 1.8 Å (Figure 3). Occasionally (e.g., *D. gigas* SI), an additional less intense longer-distance FT peak is observed at a phase-shifted distance of ca. 2.3 Å. Extraction of the FT intensity from 1.0−2.6 Å and backtransformation results in filtered EXAFS spectra, which were fit using eqs 1 and 2. Selected fits are compared to the raw data in Figure 3. Figure 4 compares filtered EXAFS and FTs of unfiltered EXAFS for all oxidation states of all the hydrogenases examined (with the exception of *A. eutrophus*; see Figure 2b,c).

Table 2 compares selected curve-fitting results for all the hydrogenase samples examined, and Tables S1−S19 in the Supporting Information provide details of all the fits attempted. For most samples, single-shell fits of the filtered Ni EXAFS reveal that the coordination sphere of nickel is dominated by S-donor ligands with average Ni−S bond distances of ca. 2.2 Å (range 2.16−2.28 Å), regardless of oxidation state. For the *D. gigas* class of enzymes (*D. gigas*, *C. vinosum*, *E. coli*), two-shell fits incorporating both S-donor and N,O-donor first-shell ligands do not show significant improvement beyond the single-shell Ni−S fits. Fits in which two shells of S-donor ligands (with Ni−S distances in the range 2.15−2.35 Å) display improvements over the single-shell fits comparable to those displayed by NiS$_x$(N,O)$_y$ fits, suggesting simply that the increase in variables is responsible for these improvements (the resulting Ni−S distances are indistinguishable with EXAFS data over

(41) Xia, J.; Dong, J.; Wang, S.; Scott, R. A.; Lindahl, P. A. *J. Am. Chem. Soc.* **1995**, *117*, 7065−7070.
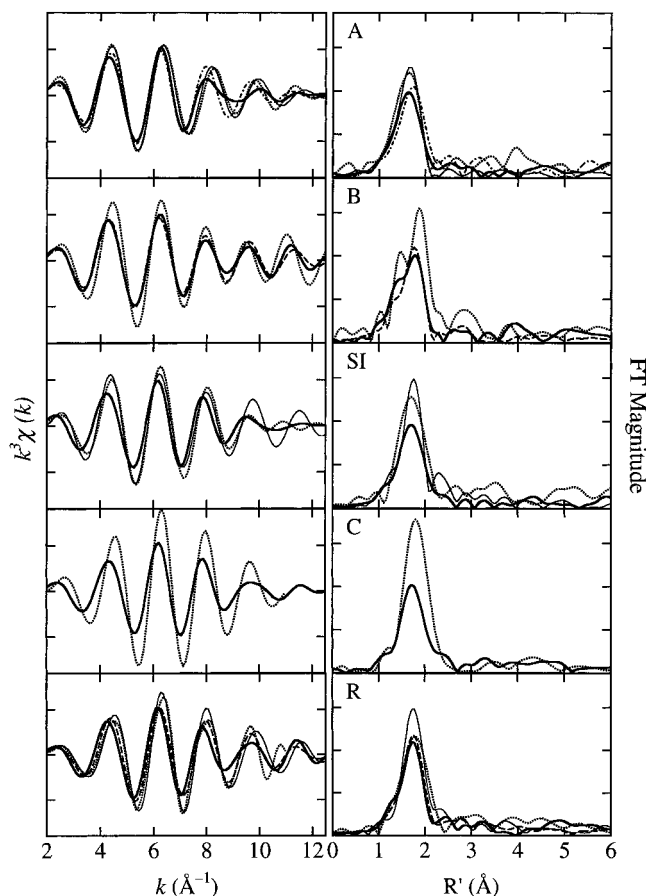
Figure 4. A comparison of the filtered EXAFS data (1.0−2.6 Å) for redox-poised samples of hydrogenases. Spectra are separated by redox level, with line types indicating different bacterial sources (see Figure 1 caption for line type definitions).

this *k* range). By contrast, two-shell fits for enzyme from *T. roseopersicina* provide evidence for N,O-donor ligands in addition to S-donor ligands. *A. eutrophus* hydrogenase is again unique in that the as-isolated form exhibits a first shell that is dominated by N,O-donor ligands. This should not be interpreted as evidence against the presence of N,O-containing ligands in the nickel coordination spheres of the *D. gigas* class of hydrogenases, since Ni−S interactions have been shown to dominate EXAFS of mixed Ni(N,O)$_x$S$_y$ ($x \leq y$) coordination spheres in model compounds, making it difficult to demonstrate the existence of Ni−(N,O) interactions by EXAFS.[35] Many of the fits in Table 2 suggest that the best-fit Ni−S coordination number is four (e.g., *D. gigas*, *C. vinosum*). Given the deduction from the edge data (*vide supra*) that the nickel site is either five- or six-coordinate, it is likely that one or two N,O-containing nickel ligands exist but do not contribute significantly to the EXAFS data.

The appearance of a small FT peak at a phase-shifted distance of ca. 2.3 Å in some of the hydrogenase Ni EXAFS suggests the presence of scattering atoms at distances of ca. 2.5−2.8 Å from the nickel site. Preliminary curve-fitting suggested the origin of this FT peak is another first-row transition metal near the nickel or is a S-containing ligand with a long Ni−S distance. When the initial crystallographic analysis of *D. gigas* hydrogenase appeared,[9] the second metal (X, likely Fe) of the dinuclear site and a long Ni−S(Cys533) bond (to one of the bridging cysteine residues) became two candidates for providing this interaction. We have subsequently conducted extensive curve-fitting of the Ni EXAFS data for all hydrogenase samples, including either Ni···Fe scattering or Ni−S scattering with

Table 2. Selected Curve-Fitting Results of Filtered EXAFS Spectra for All Hydrogenases and Model Compounds[a]

enzyme (or compound)	form	fit	n	Ni–X	R (Å)	σ^2 (×10³ Å²)	$\Delta\sigma^2$ (×10³ Å²)	correlations > 0.6	GOF
D. gigas	A	A01	5	Ni–S	2.174(1)	10.3[b](1)	7.1		0.32
		A02	4	Ni–S	2.172(1)	8.3(2)	5.1		0.46
		A03	5	Ni–S	2.174(2)	10.3(2)	7.1		0.37
			1	Ni–Fe	2.87(4)	28(6)	22		
		A04	4	Ni–S	2.177(1)	9.2(1)	6.0	$r_S/r_N = -0.64$	0.17
			1	Ni–N	1.967(3)	2.8(3)	−1.4	$r_N/\sigma_S^2 = 0.61$	
		A05	5	Ni–S	2.170(1)	12.1(1)	8.9	$r_S/r_N = -0.75$	0.14
			1	Ni–N	2.013(2)	1.9(3)	−2.5	$\sigma_S^2/\sigma_N^2 = -0.71$	
		A06	5	Ni–S	2.171(1)	12.1(1)	8.9	$r_S/r_N = -0.76$	0.11
			1	Ni–N	2.012(3)	2.0(3)	−2.4	$\sigma_S^2/\sigma_N^2 = -0.71$	
			1	Ni–Fe	2.906(14)	28.9(23)	23.4		
		A07	5	Ni–S	2.171(1)	11.8(1)	8.6	$r_S/r_N = -0.85$	0.13
			1	Ni–N	2.006(4)	2.6(4)	−1.8	$r_S/r_{Fe} = 0.71$	
			1	Ni–S	2.483(21)	39(4)	33	$\sigma_S^2/\sigma_N^2 = -0.70$	
	SI	B01	4	Ni–S	2.206(1)	6.8(1)	3.6		0.51
		B02	4	Ni–S	2.202(1)	6.3(1)	3.1		0.26
			1	Ni–Fe	2.614(2)	5.7(2)	0.2		
		B03	4	Ni–S	2.205(1)	6.9(2)	3.7		0.45
			1	Ni–S	2.769(4)	1.1(4)	−2.1		
		B04	4	Ni–S	2.203(1)	6.2(1)	3.1		0.26
			1	Ni–N	1.826(14)	24(4)	21		
			1	Ni–Fe	2.614(2)	5.5(2)	0.3		
		B05	3	Ni–S	2.199(3)	9.4(5)	6.2	$r_{S1}/r_{S2} = -0.91$	0.26
			1	Ni–S	2.203(3)	1.3(4)	−1.9	$r_{S2}/\sigma_{Fe}^2 = -0.63$	
			1	Ni–Fe	2.607(3)	5.9(3)	0.4	$r_{Fe}/\sigma_{S2}^2 = 0.63$	
								$\sigma_{S1}^2/\sigma_{S2}^2 = -0.92$	
	R	C01	5	Ni–S	2.188(3)	8.0(4)	4.8		1.29
		C02	4	Ni–S	2.189(1)	5.9(2)	2.7		0.59
		C03	4	Ni–S	2.184(2)	6.2(2)	3.0		0.61
			1	Ni–Fe	2.512(7)	7.5(6)	2.0		
		C04	4	Ni–S	2.188(1)	5.5(1)	2.3		0.53
			1	Ni–S	2.687(3)	0.6(3)	−2.6		
T. roseopersicina	A	D01	5	Ni–S	2.190(2)	11.1(3)	7.9		0.65
		D02	3	Ni–S	2.191(3)	8.9(3)	5.7	$r_S/r_N = -0.72$	0.44
			3	Ni–N	1.987(7)	8.0(9)	3.6		
		D03	3	Ni–S	2.199(3)	8.0(3)	4.8	$r_S/\sigma_N^2 = -0.64$	0.48
			2	Ni–N	1.971(6)	3.8(7)	−0.6	$r_N/\sigma_S^2 = 0.66$	
		D04	2	Ni–S	2.194(3)	5.5(3)	2.3	$r_S/\sigma_N^2 = -0.72$	0.39
			3	Ni–N	1.972(5)	5.9(6)	1.5	$r_N/\sigma_S^2 = 0.61$	
			1	Ni–Fe	2.546(7)	12.1(10)	6.6		
		D05	2	Ni–S	2.205(3)	5.3(3)	2.1	$r_{S1}/r_N = -0.70$	0.45
			3	Ni–N	1.969(4)	4.4(6)	−1.1	$r_N/\sigma_{S1}^2 = 0.65$	
			1	Ni–S	2.713(8)	7.7(11)	4.5		
	B	E01	5	Ni–S	2.213(3)	11.4(4)	7.2		0.85
		E02	4	Ni–S	2.213(4)	9.5(5)	6.3		0.98
		E03	4	Ni–S	2.234(2)	8.6(3)	5.4		0.57
			2	Ni–N	1.947(3)	0.3(4)	−4.1		
		E04	4	Ni–S	2.253(1)	10.5(3)	7.3		0.18
			2	Ni–N	1.958(1)	0.3(2)	−4.1		
			1	Ni–Fe	2.434(3)	7.7(3)	2.2		
		E05	4	Ni–S	2.240(1)	8.8(1)	5.6	$\sigma_{S1}^2/\sigma_N^2 = 0.60$	0.21
			2	Ni–N	1.950(1)	0.7(1)	−3.4		
			1	Ni–S	2.589(3)	7.4(4)	4.2		
	SI	F01	4	Ni–S	2.246(4)	10.5(6)	7.3		0.97
		F02	2	Ni–S	2.282(3)	3.4(5)	0.2	$\sigma_S^2/\sigma_N^2 = 0.62$	0.86
			3	Ni–N	1.995(4)	1.0(5)	−3.4		
		F03	4	Ni–S	2.252(5)	13.1(8)	9.9		0.87
			1	Ni–Fe	2.503(8)	6.7(9)	1.7		
		F04	4	Ni–S	2.252(3)	11.2(4)	8.0		0.83
			1	Ni–S	2.653(5)	2.1(6)	−1.1		
		F05	3	Ni–S	2.288(4)	12.2(9)	9.0	$r_{Fe}/\sigma_S^2 = 0.67$	0.41
			2	Ni–N	2.008(4)	1.0(4)	−3.4	$\sigma_S^2/\sigma_{Fe}^2 = -0.69$	
			1	Ni–Fe	2.491(4)	5.0(4)	−5.0		
		F06	3	Ni–S	2.277(2)	7.9(4)	4.7	$\sigma_{S1}^2/\sigma_N^2 = 0.64$	0.47
			2	Ni–N	1.995(3)	0.7(5)	−3.7		
			1	Ni–S	2.645(5)	3.4(7)	0.2		
	C	G01	4	Ni–S	2.213(2)	7.8(3)	4.6		0.70
		G02	4	Ni–S	2.210(2)	8.6(2)	5.4		0.43
			1	Ni–Fe	2.508(6)	9.0(6)	3.5		
		G03	4	Ni–S	2.214(1)	8.0(1)	5.8		0.36
			1	Ni–S	2.670(3)	3.8(3)	0.6		

Table 2 (Continued)

enzyme (or compound)	form	fit	n	Ni−X	R (Å)	σ^2 (×10³ Å²)	$\Delta\sigma^2$ (×10³ Å²)	correlations > 0.6	GOF
T. roseopersicina	C	G04	3	Ni−S	2.253(3)	9.8(7)	6.6	$r_{S1}/r_{S2} = -0.64$	0.29
			1	Ni−S	2.162(5)	1.6(2)	−1.6	$r_{S1}/r_{Fe} = -0.74$	
			1	Ni−Fe	2.493(3)	6.5(4)	3.3	$r_{S2}/r_{Fe} = 0.69$	
								$r_{S2}/\sigma_{S1}^2 = -0.96$	
								$r_{S2}/\sigma_{Fe}^2 = -0.68$	
								$r_{Fe}/\sigma_{S1}^2 = 0.63$	
								$\sigma_{S1}^2/\sigma_{Fe}^2 = -0.78$	
		G05	3	Ni−S	2.255(1)	4.8(2)	1.6	$r_{S1}/r_{S2} = -0.72$	0.26
			1	Ni−S	2.132(2)	0.8(3)	−2.4	$r_{S2}/\sigma_{S1}^2 = 0.86$	
			1	Ni−S	2.662(3)	5.5(4)	2.3	$\sigma_{S1}^2/\sigma_{S2}^2 = 0.85$	
	R	H01	4	Ni−S	2.235(2)	7.5(2)	4.3		0.58
		H02	4	Ni−S	2.223(2)	10.6(4)	7.4	$r_S/r_N = -0.69$	0.41
			2	Ni−N	2.095(4)	2.1(6)	−2.3	$\sigma_S^2/\sigma_N^2 = -0.82$	
		H03	3	Ni−S	2.227(1)	9.1(2)	5.9	$r_S/r_N = -0.85$	0.16
			2	Ni−N	2.079(2)	1.4(2)	−3.0	$\sigma_S^2/\sigma_N^2 = -0.85$	
			1	Ni−Fe	2.549(3)	13.5(4)	10.3		
		H04	3	Ni−S	2.237(1)	8.0(1)	4.8	$r_{S1}/r_N = -0.77$	0.20
			2	Ni−N	2.064(2)	2.3(2)	−2.1	$\sigma_{S1}^2/\sigma_N^2 = -0.62$	
			1	Ni−S	2.728(4)	10.0(5)	6.8		
C. vinosum	A	J01	5	Ni−S	2.172(2)	10.5(3)	7.3		0.64
		J02	4	Ni−S	2.172(2)	8.5(3)	5.3		0.78
		J03	3	Ni−S	2.188(1)	5.8(2)	2.6		0.33
			2	Ni−N	1.914(3)	2.0(4)	−2.4		
		J04	3	Ni−S	2.187(1)	5.6(1)	2.4		0.17
			2	Ni−N	1.912(1)	1.8(2)	−2.6		
			1	Ni−Fe	2.689(5)	16.3(7)	10.8		
		J05	3	Ni−S	2.187(1)	5.9(1)	2.7		0.23
			2	Ni−N	1.915(2)	2.2(3)	−2.2		
			1	Ni−S	2.702(7)	4.0(9)	0.8		
	B	K01	5	Ni−S	2.208(3)	9.1(5)	5.9		1.20
		K02	4	Ni−S	2.219(2)	6.0(3)	3.8		0.94
			2	Ni−N	1.886(6)	1.4(7)	−3.0		
		K03	4	Ni−S	2.221(3)	7.7(4)	4.5		0.73
			2	Ni−N	1.883(6)	3.3(8)	−1.1		
			1	Ni−Fe	2.466(7)	7.0(9)	1.5		
		K04	4	Ni−S	2.221(2)	6.4(3)	3.2		0.82
			2	Ni−N	1.885(6)	2.1(7)	−2.3		
			1	Ni−S	2.630(8)	3.3(9)	0.1		
	SI	L01	5	Ni−S	2.200(2)	9.7(3)	6.5		0.72
		L02	4	Ni−S	2.200(3)	7.9(3)	4.7		0.84
		L03	4	Ni−S	2.196(3)	8.6(3)	5.4		0.68
			1	Ni−Fe	2.507(8)	8.4(9)	2.9		
		L04	4	Ni−S	2.202(3)	8.1(4)	4.9		0.87
			1	Ni−S	2.673(14)	7.0(19)	3.8		
		L05	3	Ni−S	2.142(1)	3.3(2)	0.1	$r_{S1}/r_{S2} = 0.62$	0.42
			2	Ni−S	2.286(2)	0.6(2)	−2.6	$\sigma_{S1}^2/\sigma_{S2}^2 = 0.86$	
		L06	3	Ni−S	2.146(2)	3.4(3)	0.2	$r_{S1}/r_{S2} = 0.81$	0.44
			2	Ni−S	2.290(3)	0.7(4)	−2.5	$r_{S1}/\sigma_{Fe}^2 = -0.69$	
			1	Ni−Fe	2.420(29)	24(6)	18	$r_{S2}/\sigma_{Fe}^2 = -0.68$	
								$r_{Fe}/\sigma_{S2}^2 = 0.65$	
								$\sigma_{S1}^2/\sigma_{S2}^2 = 0.92$	
		L07	3	Ni−S	2.144(2)	3.3(2)	0.1	$r_{S1}/r_{S2} = 0.66$	0.40
			2	Ni−S	2.289(2)	0.7(3)	−2.5	$\sigma_{S1}^2/\sigma_{S2}^2 = 0.88$	
			1	Ni−S	2.649(24)	23(5)	20		
	C	M01	4	Ni−S	2.209(2)	4.2(2)	1.0		1.22
		M02	4	Ni−S	2.202(1)	3.6(1)	0.4		0.41
			1	Ni−Fe	2.539(2)	3.4(3)	−2.1		
		M03	4	Ni−S	2.209(1)	4.1(1)	0.9		0.58
			2	Ni−S	2.691(3)	4.1(3)	0.9		
	R	N01	4	Ni−S	2.203(3)	6.8(3)	3.6		0.90
		N02	4	Ni−S	2.203(1)	7.9(2)	4.7		0.39
			1	Ni−Fe	2.462(5)	9.6(6)	4.1		
		N03	4	Ni−S	2.203(1)	7.0(1)	3.8		0.35
			1	Ni−S	2.645(5)	5.6(6)	2.4		
		N04	2	Ni−S	2.159(3)	9.9(6)	6.7		0.20
			2	Ni−S	2.220(2)	2.1(1)	−1.1		
			1	Ni−S	2.660(2)	3.3(3)	0.1		
D. desulfuricans	B	P02	4	Ni−S	2.220(1)	9.1(1)	5.9		0.28
		P04	3	Ni−S	2.226(1)	6.4(1)	3.2		0.21
			1	Ni−N	1.928(4)	5.9(6)	1.5		
		P05	3	Ni−S	2.225(1)	6.3(1)	3.1		0.22
			1	Ni−N	1.923(5)	5.5(8)	1.1		
			1	Ni−Fe	2.721(14)	24.5(23)	19.0		

Table 2 (Continued)

enzyme (or compound)	form	fit	n	Ni–X	R (Å)	σ^2 (×10³ Å²)	$\Delta\sigma^2$ (×10³ Å²)	correlations > 0.6	GOF
D. desulfuricans	B	P06	3	Ni–S	2.225(1)	6.4(1)	3.2		0.20
			1	Ni–N	1.927(5)	6.0(8)	1.4		
			1	Ni–N	2.736(14)	14.3(26)	11.1		
	R	Q02	4	Ni–S	2.211(1)	8.1(1)	4.9		0.41
		Q03	4	Ni–S	2.216(1)	8.7(2)	5.5	$\sigma_S^2/\sigma_{Fe}^2 = -0.62$	0.35
			1	Ni–Fe	2.452(8)	16.9(13)	11.4		
		Q04	4	Ni–S	2.214(7)	8.3(1)	5.1		0.28
			1	Ni–S	2.647(5)	10.5(7)	7.3		
		Q05	3	Ni–S	2.256(2)	12.1(5)	8.9	$r_{S1}/r_{Fe} = 0.70$	0.13
			1	Ni–S	2.175(2)	1.7(2)	-1.5	$\sigma_{S2}^2/\sigma_{S1}^2 = 0.87$	
			1	Ni–Fe	2.478(3)	8.9(3)	3.7	$\sigma_{S2}^2/\sigma_{Fe}^2 = 0.77$	
		Q06	3	Ni–S	2.246(2)	8.6(4)	5.4	$r_{S1}/r_{S2} = -0.78$	0.13
			1	Ni–S	2.167(4)	2.9(2)	-0.3	$r_{S1}/\sigma_{S1}^2 = -0.72$	
			1	Ni–S	2.644(3)	8.0(4)	4.8	$r_{S1}/\sigma_{S2}^2 = -0.72$	
E. coli	A	R01	5	Ni–S	2.208(1)	11.6(2)	8.4		0.53
		R02	5	Ni–S	2.215(2)	13.1(2)	9.9		0.40
			1	Ni–Fe	2.458(5)	11.2(7)	5.7		
		R03	5	Ni–S	2.213(1)	12.0(2)	8.8		0.34
			1	Ni–S	2.633(4)	6.1(5)	2.9		
		R04	3	Ni–S	2.214(4)	8.6(4)	5.4	$r_S/\sigma_N^2 = -0.73$	0.55
			1	Ni–N	1.965(13)	4.8(19)	0.4		
			1	Ni–Fe	2.493(7)	10.2(8)	4.7		
A. eutrophus	as-isol	S01	5	Ni–N	2.094(4)	4.7(5)	0.3		1.16
		S02	2	Ni–S	2.359(4)	7.3(5)	4.1		0.66
			4	Ni–N	2.068(2)	2.6(3)	-1.8		
		S03	3	Ni–S	2.349(2)	9.9(4)	6.7		0.47
			3	Ni–N	2.063(2)	1.3(2)	-3.1		
			1	Ni–Fe	2.857(7)	10.1(9)	4.6		
		S04	3	Ni–S	2.340(3)	6.6(5)	3.4	$r_{S1}/r_{S2} = 0.80$	0.55
			3	Ni–N	2.052(2)	0.5(3)	-3.9	$\sigma_{S1}^2/\sigma_N^2 = 0.73$	
			1	Ni–S	2.538(8)	5.1(12)	1.3	$\sigma_{S1}^2/\sigma_{S2}^2 = 0.87$	
								$\sigma_N^2/\sigma_{S2}^2 = 0.61$	
	red	T01	4	Ni–S	2.195(1)	3.9(2)	0.7		0.98
		T02	4	Ni–S	2.193(1)	4.4(1)	1.2		0.60
			1	Ni–Fe	2.462(5)	7.8(6)	2.3		
		T03	4	Ni–S	2.195(1)	3.8(1)	0.6		
			1	Ni–S	2.639(3)	3.1(4)	-0.1		
		T04	3	Ni–S	2.197(1)	1.8(1)	-1.4		0.45
			1	Ni–N	1.932(10)	5.7(17)	1.3		
			1	Ni–S	2.645(3)	1.4(4)	-1.8		
Ni(cyclam)(SPh)$_2$		U01	4	Ni–N	2.062(3)	2.1(3)	-2.3		0.52
			2	Ni–S	2.564(3)	3.2(4)	0		
		U02	4	Ni–N	2.073(7)	4.3(8)	-0.1		1.16
			1	Ni–Fe	2.407(6)	3.8(9)	-1.7		
		U03	4	Ni–N	2.063(1)	2.1(2)	-2.3		0.33
			2	Ni–S	2.566(2)	3.5(2)	0.3		
			8	Ni–C	2.93(1)	23.6(21)			
		U04	4	Ni–N	2.075(4)	4.5(6)	1		0.76
			1	Ni–Fe	2.407(4)	3.9(4)	-16		
			8	Ni–C	2.93(1)	10			
calculated data		V01	4	Ni–S	2.216(1)	3.4(1)	0.2	$r_{Fe}/\sigma_{S2}^2 = -0.99$	
			1	Ni–Fe	2.66(3)	9.1(9)	3.6		0.41
			1	Ni–S	2.71(2)	8 (9)	4.8	$r_{S2}/\sigma_{Fe}^2 = 0.84$	
		V02	4	Ni–S	2.215(1)	3.3(1)	0.1		0.47
			1	Ni–Fe	2.630(5)	9.3(6)	3.8		
		V03	4	Ni–S	2.216(1)	3.5(1)	0.3		0.36
			1	Ni–S	2.798(3)	3.6(3)	0.4		

[a] X is the scattering atom for each shell; R is the Ni–X distance; σ^2 is the root mean square disorder in Ni–X distance; $\Delta\sigma^2$ is σ^2 relative to reference compounds; correlations lists all parameter cross-correlations with absolute values of 0.6 or greater; GOF is the goodness-of-fit defined in the Experimental Section. [b] Underlined values are approaching physical insignificance. Large values of σ^2 suggest that the shell involved has a coordination number that is too large or is badly disordered and may be unnecessary for fitting the data.

distances in the 2.4–2.9 Å range. These fits are detailed in Tables S1–S19, and selected examples are included in Table 2.

The difficulty in distinguishing Ni–S from Ni···Fe scattering is illustrated by the analysis of data from a model compound, [Ni(cyclam)(SPh)$_2$], in Figure 5a. This compound has two thiophenolates axially coordinated at 2.6 Å distances to Ni(II), with equatorial coordination sites occupied by the tetraaza macrocycle cyclam.[42] Figure 5a compares a fit including 4 Ni–N and 2 Ni–S at the crystallographically determined distances with a fit including 4 Ni–N and 1 Ni···Fe (see Table 2 for details of fits). Although the latter (incorrect) fit looks worse than the correct one, the difference is not large and with lower quality data (as is typical for metalloenzymes), these fits would be nearly indistinguishable.

Analysis of the Ni EXAFS of the *D. gigas* and *E. coli* form A hydrogenases provides no support for any scattering in the

(42) Waden, H.; Seak, W.; Haase, D.; Pohl, S. *Angew. Chem.*, in press.
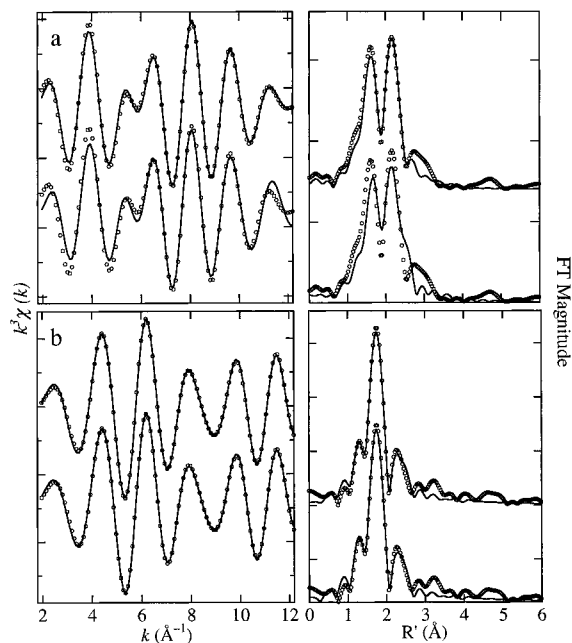
Figure 5. (a) Ni K-edge filtered (1.0–2.6 Å) and Fourier-transformed EXAFS spectra for Ni(cyclam)(SPh)$_2$. The upper spectra show the data (open circles) and a fit (solid line) incorporating two axial S-donor atoms (4 N at 2.06 Å, 2 S at 2.57 Å, Table 2 fit U03). The lower spectra illustrate the data and fit generated by substituting an Fe atom for the long S-donor atoms (4 N at 2.08 Å, 1 Fe at 2.40 Å, Table 2 fit U04). (b) A comparison of the *D. gigas* filtered (1.0–2.6 Å) EXAFS data (open circles) for SI with fits employing an outer shell of either Fe (top, 4 S at 2.20 Å, 1 Fe at 2.61 Å, Table 2 fit B02) or S (bottom, 4 S at 2.21 Å, 1 S at 2.77 Å, Table 2 fit B03).

2.4–2.9 Å range, whereas analysis of form A of *T. roseopersicina* and *C. vinosum* allows the presence of a single 2.7 Å Ni–S interaction. Attempts to assign one Fe scatterer to this EXAFS component resulted in unrealistically large Debye–Waller σ^2 values (Table 2). This problem could be eliminated if the Fe site is assumed to be fractionally occupied or if the Ni site is assumed to be heterogeneous in Ni⋯Fe separation. Of the form B samples examined, only *T. roseopersicina* hydrogenase exhibits a significant improvement in the fit upon addition of Ni⋯Fe (at 2.44 Å) or Ni–S (at 2.60 Å). The improvement for *C. vinosum* was insignificant and no improvement was observed for *D. desulfuricans*. The results for the reduced forms (SI, form C, R) are more consistently supportive of the presence of long-distance interactions. Only the SI sample of *C. vinosum* and the R sample of *D. gigas* show insignificant (less than a factor of two) improvement in the goodness of fit value over the corresponding fit without the long-distance interaction. In most cases, either Ni⋯Fe (with distances ranging from 2.46 to 2.61 Å) or Ni–S (with distances ranging from 2.64 to 2.77 Å) provide similar improvements. The single exception is the SI sample of *D. gigas* hydrogenase, for which the fit with Ni⋯Fe (at 2.61 Å) is 1.7 times better than the fit with a long Ni–S (at 2.77 Å). However, Figure 5b shows that it is still difficult to distinguish these two fits. The data quality do not support attempts to evaluate whether this long-distance feature might arise from a combination of both Ni⋯Fe and long Ni–S, although this is likely taking the crystallographic data at face value (*vide infra*).

Figure 2 shows that the Ni EXAFS for the *A. eutrophus* hydrogenase are qualitatively different from those for the other hydrogenases examined. The lower intensity and shorter distance for the FT peak of the as-isolated sample suggest that the proportion of N,O-containing ligands has increased, in agreement with interpretation of the XANES (vide supra).

Results of curve-fitting of the Ni EXAFS confirm this, suggesting an average nickel coordination environment of Ni(N,O)$_{3-4}$S$_{3-2}$ (Table 2). The average Ni–S distances also appear longer than those obtained for the other hydrogenases: 2.36 Å compared with ca. 2.2 Å. Consistent with the large change in the XANES upon reduction (with NADH and H$_2$; see the Experimental Section), a large change in the EXAFS-derived first coordination sphere is also observed. The NADH- and H$_2$-reduced sample displays a nickel coordination environment similar to the other hydrogenases. It is now dominated by Ni–S with ca. 2.2 Å distances and the data support the presence of a long-distance interaction that can be fit with either Ni⋯Fe at 2.46 Å or with Ni–S at 2.64 Å. Apparently, a significant structural rearrangement occurs at the nickel site during reductive activation of this enzyme.

Our results on the *D. gigas* hydrogenase are in general agreement with the published crystallographic analysis.[9] The crystallographic results were obtained on a mixture of EPR-active and -silent forms of the enzyme; we must therefore consider the long-distance interaction observed in the EXAFS of the SI form in comparisons. The EXAFS-derived first-shell Ni–S distances (2.20 Å) are shorter than the average of the three shorter crystallographic Ni–S distances (2.25 Å), but this agreement is well within the crystallographic error. One long (2.6 Å) Ni–S bond to the bridging Cys533 was observed in the crystallographic analysis and the second metal, X, was suggested to be ca. 2.7 Å away from the nickel. The long-distance interaction observed in the EXAFS could arise from three distinct possibilities. First, the EXAFS observed could be solely the result of long (2.77 Å) Ni–S bonds (to one or perhaps both bridging cysteines). This explanation would require that either the Ni⋯Fe distance is substantially longer than the ca. 2.7 Å estimate from the crystallographic analysis, or that the Ni⋯Fe distance is sufficiently heterogeneous in frozen samples that the EXAFS arising from the second metal is not observed. Second, the observed EXAFS could result solely from scattering from the other metal center, such as an Fe atom at 2.61 Å. This explanation implies that the crystallographically determined 2.6 Å Ni–S(Cys533) distance is somewhat overestimated, such that the EXAFS does not distinguish it from the first-shell Ni–S interactions, or that it is badly disordered. This explanation is supported by the fact that most of the fits, particularly to reduced enzymes, show a preference for four ~2.2 Å Ni–S distances. Taking the crystallographic results at face value, it is likely that the observed EXAFS is the sum of scattering interactions arising from both a long S-donor and a neighboring metal atom. This third explanation requires no significant modification of the distances obtained from the crystal structure, and has the highly desirable feature that the absence of peaks attributable to scattering atoms at a longer distance in the Fourier transforms of most samples, and the presence of such peaks in other samples, can be readily explained.

As shown in Figure 6, holding the structure of the Ni site constant with three normal and one long Ni–S distances while varying the Ni⋯Fe distance, leads to calculated EXAFS spectra that exhibit the appearance and disappearance of a peak corresponding to the long distance scattering atoms in the Fourier-transformed spectra of the enzymes. When the Ni–S and Ni⋯Fe distances are similar, no peak is observed because the EXAFS arising from Ni–S and Ni-Fe vectors at comparable distances are in destructive interference with each other. (The same effect can be generated by holding the Ni⋯Fe distance constant and varying the Ni–S distance.) This is exactly the situation that would be expected given the crystallographic
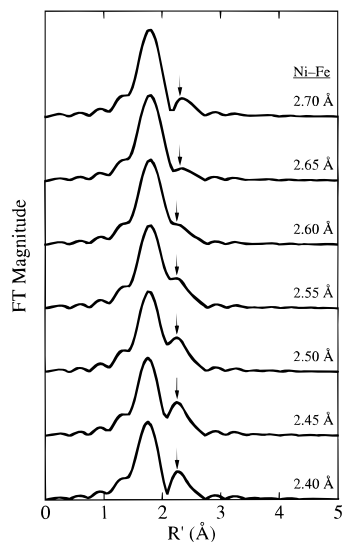
Figure 6. Theoretical EXAFS spectra calculated for 3 S at 2.25 Å and 1 S at 2.60 Å and a variable Ni−Fe distance, 2.40−2.70 Å.

distances. Thus, the observation of a peak in one case and the absence of a peak in another case could be attributed to a variation of Ni···Fe or long Ni−S distances in different enzymes or upon a change in redox poise. This explanation has the unfortunate consequence that the distance determined by fitting the long scattering atoms with either S or Fe reflects neither distance in the enzyme, since the net EXAFS is the sum of the two components. For example, if the calculated EXAFS data for a Ni···Fe distance of 2.70 Å (3 S at 2.25 Å + 1 S at 2.60 Å + 1 Fe at 2.70 Å) are treated as experimental data, fits for a single Fe scatterer (4 S at 2.21 Å + 1 Fe at 2.63 Å; GOF = 0.47), a single S scatterer (4 S at 2.22 Å + 1 S at 2.80 Å; GOF = 0.36), and for both (4 S at 2.22 Å + 1 Fe at 2.66 Å + 1 S at 2.71 Å; GOF = 0.41) may be compared (Table 2, fits V01−V03). The fit obtained for the single S scattering atom has the lowest GOF value, but the Ni−S distance obtained is 0.2 Å longer than the true value. Similarly, when Fe alone is used to fit the data, the distance obtained is substantially shorter than the true distance. Employing both scattering atoms does not improve the goodness of fit and so would not be considered among the best fits.

Conclusions

Our comparison of Ni XAS results on a number of [NiFe]-hydrogenases has allowed us to focus on the common aspects of the nickel-site structures in this enzyme class. Some general conclusions can be drawn from this comparison. First, the Ni K-edge energy variation with enzyme oxidation state change (ca. 1 eV, less than an electron) suggests that a slight increase in electron density occurs at the nickel during reduction from the inactive oxidized forms (form A, form B) to the SI state. Further reduction to form C and R involves virtually no change in electron density at the nickel. Second, a coordination change occurs from five- to six-coordination upon the reduction to SI for all the enzymes except that from *T. roseopersicina*. This change in coordination may be responsible for a significant

fraction of the edge energy shift since the shift is less for the *T. roseopersicina* enzyme. In the *A. eutrophus* enzyme, the changes that occur upon reduction by NADH and H_2 are different, converting a sulfur-deficient nickel site into a site more like the other hydrogenases. Third, analysis of the Ni EXAFS provides evidence for dominant sulfur ligation involving ca. four S-donor ligands in the first-shell coordination sphere of Ni in all oxidation states for all enzymes (except as-isolated *A. eutrophus*). The nickel site of the *T. roseopersicina* enzyme appears to have a higher proportion of N,O-containing ligands than S-containing ligands compared to the other enzymes. Although there is often no EXAFS evidence for N,O-containing ligands, the five- or six-coordinate site dictated by the XANES data strongly suggests the presence of one or two undetected N,O-containing ligands. One of these may be the potential third bridging ligand, I, reported in the crystallographic analysis of the *D. gigas* enzyme.[9] It is unlikely that I is a μ-oxo bridge, since there is no EXAFS evidence for a short (1.7−1.8 Å) Ni−O distance; μ-hydroxo, μ-aquo, and similar bridges remain possibilities. Fourth, the EXAFS provides evidence for a long-distance scatterer, predominantly in the more reduced enzymes (SI, form C, and R), that could result from one or more long (2.64−2.77 Å) Ni−S bonds (e.g., to the bridging cysteines of the *D. gigas* crystallographic model), from a (2.46−2.61 Å) Ni···X interaction (where X is a first-row transition metal), or from a combination of these features.

Supporting Information Available: Tables S1−S19 of fits of Ni K-edge Fourier-filtered EXAFS data (back-transform window 1.0−2.6 Å, uncorrected) for the hydrogenase samples featured in this paper (74 pages). See any current masthead page for ordering and Internet access instructions.

JA962429P